Flow Field Study on a Supercritical Airfoil Using a Pressure Probe and a Two-component Laser-Doppler-Anemometer

Karl A. Bütefisch and E. Stanewsky

Deutsche Forschungs- und Versuchsanstalt für
Luft und Raumfahrt e.V.
Institut für Experimentelle Strömungsmechanik
34 Göttingen, Germany

ABSTRACT

The aim of this study was the investigation of the phenomenon of shock boundary layer interaction on a supercritical airfoil with and without shock-induced separation and a comparison of results obtained by conventional boundary layer probe and a two component Laser Doppler Anemometer. Measurements were made in the 1 x 1 m^2 Transonic Wind Tunnel (TWG) of the DFVLR Göttingen on a 250 mm chord model of the airfoil CAST 7/DOA1 at a Mach number of $M_\infty = 0.765$ and angles of attack of $\alpha = 3.6°$ and $4.8°$. The Reynolds number was $Re = 2.5 \times 10^6$

Nomenclature

b	test section width, model span
c	airfoil chord
c_f	skin friction coefficient
C_L	lift coefficient
c_p	pressure coefficient, $(p-p_\infty)/q_\infty$
H	shape parameter, δ^*/θ
	distance from wall in LDA results
H_{32}	shape parameter, δ^{**}/θ
M	Mach number
p	static pressure
q	dynamic pressure
Re	Reynolds number, $U_\infty c/\nu_\infty$
u	velocity in the boundary layer
u_τ	friction velocity, $(\tau_w/\rho_w)^{1/2}$
U^+	velocity based on law of the wall, u/u_τ
U_∞	freestream velocity
x	coordinate in streamwise or chord direction
y	coordinate normal to streamwise direction or normal to model surface in boundary layer measurements
Y^+	$y\, u/u_\tau$
δ	boundary layer thickness
δ^*	displacement thickness
δ^{**}	energy thickness
θ	momentum thickness
ν	kinematic viscosity
ρ	density
τ	shear stress

Subscripts

e	edge of boundary layer
L	local conditions
w	wall
∞	freestream conditions

1 upstream of shock

1. INTRODUCTION

There is certainly no need to stress here the importance of the investigation of transonic flow fields to the development and design of aerodynamic flight vehicles and their components. Such flow fields may occur on transonic airfoils and wings of transport and fighter aircraft, on helicopter blades, in turbomachinery and in the recompression region of supersonic intakes. One characteristic feature of these flow fields, at least at off-design conditions, is the interaction between a near normal shock wave, terminating the local supersonic region, and the boundary layer. The severety of this interaction determines in many instances the performance boundaries of a flight vehicle and it is therefore not surprising that a considerable interest in details of this flow phenomenon and means of its control exist [1].

Since theoretical methods are not yet able to treat the overall shock boundary layer interaction satisfactorily, one must strongly rely on experimental results for the qualitative and quantitative assessment of the associated flow development. This is particularly true with regard to shock induced separation and the generation and/or amplification of turbulence within the interaction region. Providing the needed information requires, of course, a continuous effort is developing adequate tools. It is in that sense that a thorough investigation of the interaction field by boundary layer probe measurements, essentially providing rather gobal information [2], was followed by tests with a one-component Laser-Doppler-Anemometer [3]. Here, the initial aim was to determine the suitability of the instrumentation for the quantitative analyses of transonic shock boundary layer interaction in a relatively large wind tunnel. The present study is a continuation of these efforts with an LDA-system that differs from the former in that (a) a two-component Laser-Doppler-Anemometer is employed and (b) this system operates in a back-scattering mode where the signal intensities are less, which allows, however, the investigation of complex three-dimensional configurations. The test cases are the same in both instances providing a comparison of two modes of LDA-operation and conventional boundary layer probe measurements.

2. EXPERIMENTAL SET-UP AND TEST CONDITIONS

2.1 Wind Tunnel

The Transonic Wind Tunnel Göttingen TWG, [4] is a continuous closed circuit tunnel with two test sections in series. The transonic test section, of concern here, operates in a Mach number range between M_∞ = 0.50 to 1.20 at total pressures ranging from 0.25 to 1.6 bar, the latter allowing the Reynolds number to be varied between $Re/c \simeq 3 \times 10^6$ to 20×10^6 m^{-1}. The test section has a cross section of 1m × 1m and consists of four perforated walls with 30-degree slanted holes and an open area ratio of 6 percent. It is enclosed in a plenum of about 8 meters diameter which housed, as will be discussed later, the present LDA-system. Upstream of the transonic test section is the flexible supersonic nozzle and the settling chamber, the latter containing the probe for seeding the flow, Fig. 1.

2.2 Airfoil and Model Arrangement

The present investigation was carried out utilizing the transonic airfoil CAST 7/DOA1, designed by the Dornier Company, which has previously been used extensively for similar studies [2][3]. The airfoil is shock-free at the design point M_∞ = 0.760, C_L = 0.573. It is, furthermore, characterized by a moderate rear loading and a relatively small trailing edge angle, Fig. 2. Details concerning the airfoil and the design process can be found in Ref. 5 and 6.

The arrangement of the model in the tran-

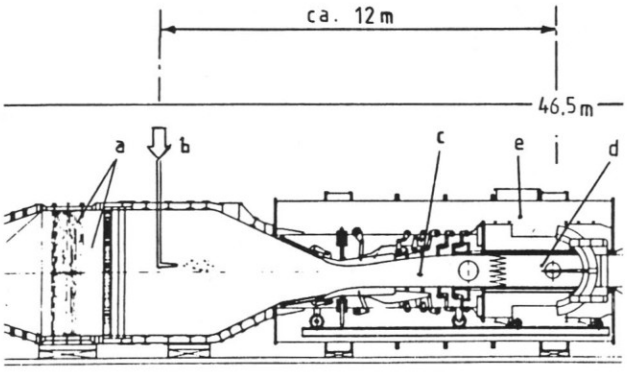

a. Settling chamber with cooler, screens and honeycombs. b. Seeding probe. c. Supersonic nozzle. d. Transonic test section. e. Plenum chamber.

Fig. 1: Transonic Wind Tunnel Göttingen (TWG).

sonic test section of TWG is shown in Fig. 3 - here with the boundary layer probe and probe support installed. The model, with a chord of c = 250 mm, spanned the entire width of the tunnel providing a span to chord ratio of b/c = 5 which rendered the test set-up essentially free of side wall interference effects. The model was supported by rotatable discs, embedded in the side walls, consisting of two parts, the upper one made of Schlieren glass, the lower one of steel to carry the model loads. The Schlieren windows allow the observation of the entire upper surface as well as the nose and trailing edge region of the lower side. The model was equipped with 117 orifices for surface pressure measurements.

2.3 Test Conditions

For the present study two off-design cases were selected, one with a shock-upstream Mach number of $M_1 \approx 1.30$ where shock induced separation is incipient, and a second with

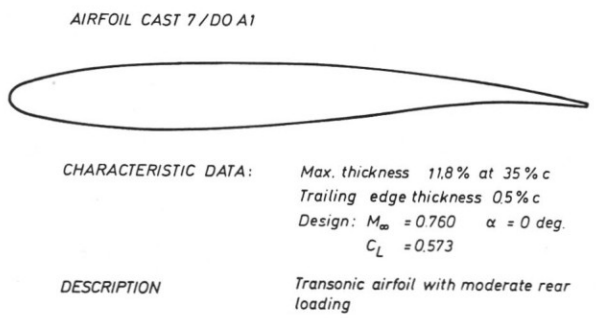

Fig. 2: The airfoil investigated.

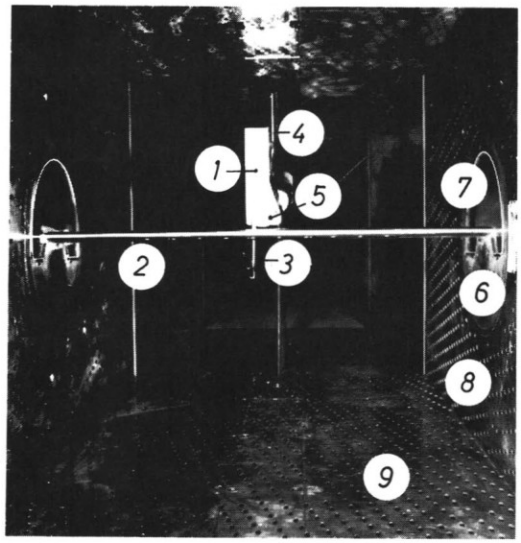

① DRIVE UNIT ENCASEMENT ② AIRFOIL MODEL
③ PROBE SUPPORT ④ STING SUPPORT ⑤ STING
⑥ ROTATABLE WALL INSERT TO VARY α
⑦ SCHLIEREN WINDOW ⑧ STEEL INSERT TO CARRY MODEL LOADS ⑨ PERFORATED (6% OPEN) TEST SECTION WALLS

Fig. 3: Model installation - here with boundary layer probe and support system - in the Transonic Wind Tunnel Göttingen (TWG).

a shock-upstream Mach number of $M_1 \approx 1.36$ where substantial separation occurs. Representative upper surface Mach number distributions are shown in Fig. 4, Schlieren pictures, also indicating the flow field investigated, are presented in Fig. 5. Concerning the Mach number distributions, the following remarks are deemed necessary. The probe and its support (see Fig. 3) were removed from the test section for the LDA-measurements. Especially the probe support caused at the lower angle of attack, $\alpha = 3.5°$, some global interference resulting mainly in a difference in the shock location between the probe and the LDA set-up, Fig. 4a. Subsequent comparisons between the probe and the LDA data will therefore be made relative to the shock location. At the higher angle of attack, $\alpha = 5°$, only a slight difference in the rear pressure recovery exists, Fig. 4b. The slight difference in the angles of incidence are due to matching the lift coefficient for the two sets of measurements.

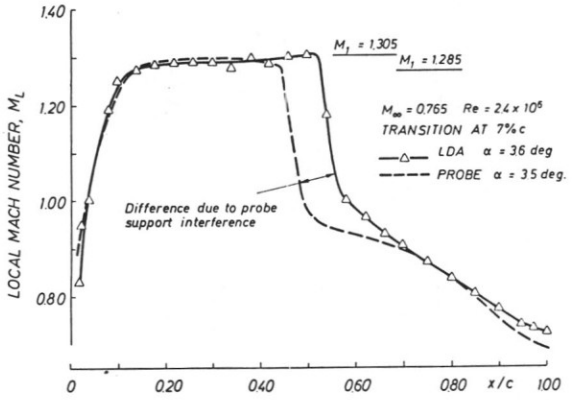

Fig. 4a: Upper surface Mach number distributions at moderate incidence.
$\alpha \approx 3.5$ deg., $M_1 \approx 1.29$.

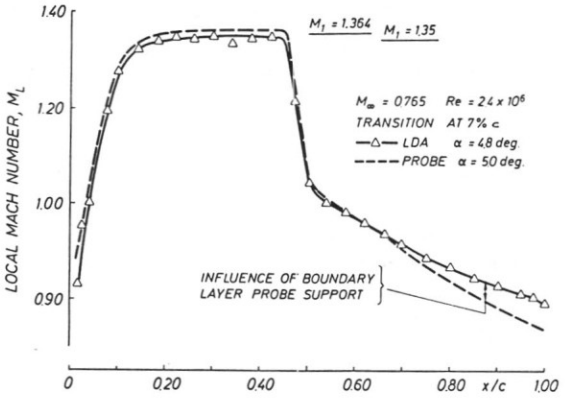

Fig. 4b: Upper surface Mach number distributions at high incidence.
$\alpha \approx 5$ deg., $M_1 \approx 1.35$.

3. LASER DOPPLER ANEMOMETER AND BOUNDARY LAYER PROBE

3.1 Laser Doppler Anemometer

The LDA system was designed for application in large wind tunnels and has to fulfill the requirements given by the rough environment of large facilities. For the present investigation a commercial two component LDA system (TSI 9100) was available, but had to be adapted to the special tunnel (TWG) requirements such as:

- Large measuring distance of 750 mm
- Accurate positioning with a spatial resolution of 0.012 mm
- Installation in the plenum chamber of the wind tunnel TWG

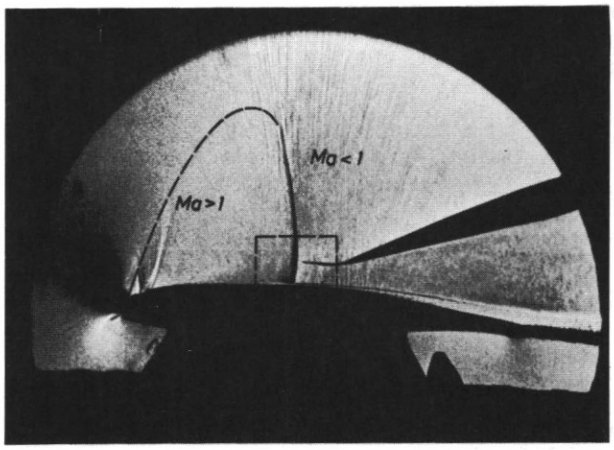

Fig. 5: Flow field of the test cases investigated. $\alpha = 3.6°$ and $4.8°$.

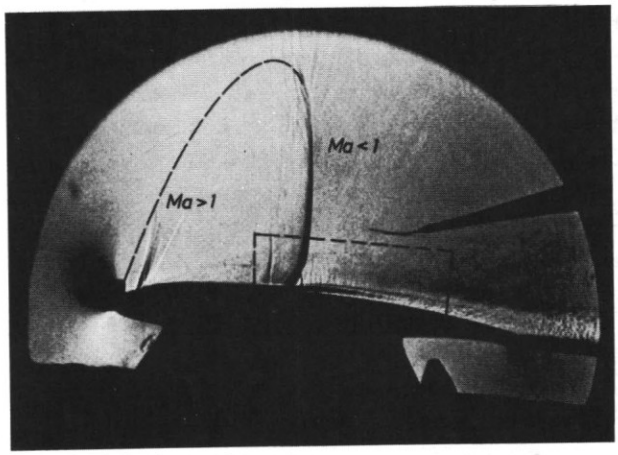

- Quick installation
- Realignement of optics and laser by remote control during tunnel operation due to pressure changes in the plenum chamber
- Fully automatic operation during a wind tunnel run including
  - Quick positioning of the measuring volume
  - Quick data acquisition and reduction
  - Quick - look results
- Insensitivity to mechanical vibrations and a high noise level

To meet these requirements, an LDA system to be operated in the backscattering mode was chosen. After some initial measurements in a fully turbulent pipe flow and in the 3x3 m^2 low speed wind tunnel (NWG) of the DFVLR at Göttingen [9], the present survey of the flow field surrounding a supercritical arofoil was the first application in the transonic range.

Fig. 6 shows schematically the optical system of the 750 mm dual beam LDA. The green and blue lines of an argon ion laser are directed via mirrors onto beam splitters to form two pairs of parallel laser beams of equal intensity. Passing the transmitting optics they intersect each other in a distance of 750 mm.

Small oil particles of about 1 µ diameter, crossing the point of intersection (measuring volume) with the surrounding flow velocity, scatter partially the light. The same lenses used for transmitting the laser beams are collecting the scattered light which is Doppler shifted due to the motion of the particles. The scattered light is passed to photomultipliers where the Doppler frequencies, proportional to the velocity of the particles, are obtained as electrical signals. Counters convert the analog signals into digital data which are processed by a minicomputer DEC-PDP 11/24. All optical parts were commercially acquired. However, the receiving modules had to be modified to optimize the alignment. This was accomplished by small servo-motors operated by remote control. To avoid additional mirrors, the optical axis was chosen to be nearly perpendicular to the mean flow direction in the test section. Due to the geometric constraints in the plenum chamber of the tunnel, Fig. 1, the overall set-up was limited to a total length of 1.40 m which was also the minimum length given by the 4 W argon ion laser (Spectra Physics Mod. 165). As shown in Fig. 7, the two optical systems with their common focal point forming the measuring volume within the flow field were installed together on a rigid X-beam construction, [10]. For each color one leg served as the emitting and the other as the receiving device. The advantages of this set-up compared to an on-axis system are the reduction unwanted scattered light and the decrease of the effective length of the measuring volume. Especially measurements in the vicinity of a wall suffer from scattered light and hence an increase of artifical "turbulence". Of course, the main disadvantage of the backscatter operation, i.e., the lower light intensity, still remains.

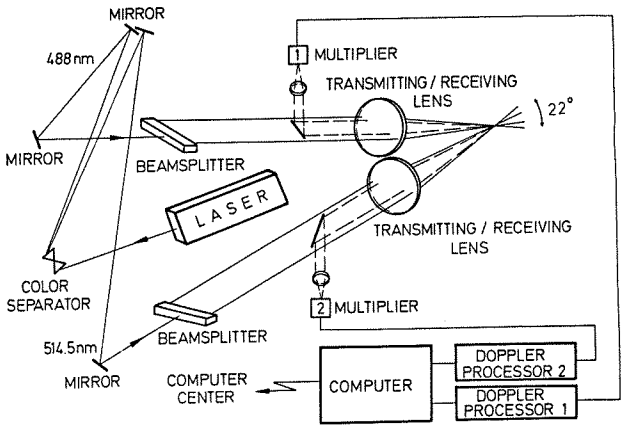

Fig. 6: Schematical view of the 750 mm two component dual beam laser Doppler anemometer.

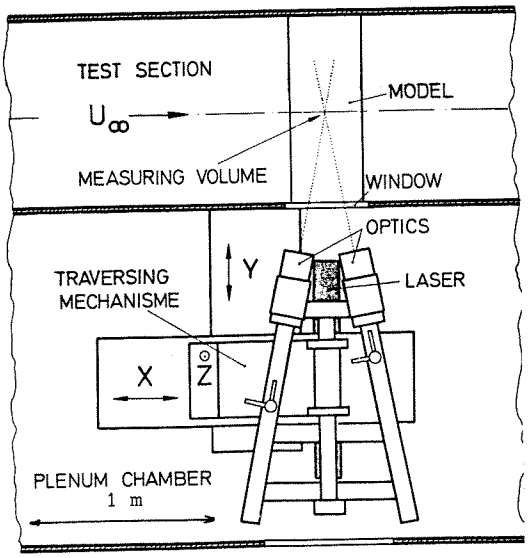

Fig. 7: LDA set-up installation in the plenum chamber of the Transonic Wind Tunnel Göttingen (TWG).

The whole optical system was mounted on a coordinate table to permit traversing along the three coordinate axes (1m x 1m x 0.5m) in steps of 1/80mm. A micro processor for each coordinate and an additional processor as supervisor and interface device to the main computer (PDP 11/24) allowed the accurate positioning of the measuring volume along diagonals in space. A maximum traversing speed of about 100mm/s was possible. The specific measuring stations, where data were to be collected during a run, were preselected and stored in the computer before measurements took place. Controlled by the main computer, positioning, data collect-

ing and the computations of quick-look-results were performed automatically [9].
It is well known that the calculated mean velocity value representing a certain number of individual measurements may be influenced by the averaging procedure [11,12]. Simple arithmetic averaging, and in addition, velocity weighted averaging were used to obtain the mean velocity values from about 1000 samples per component. The data rate was chosen to be about 200 samples/s leading to a measuring time of about 5 s per acquired field point. This seemed to be an appropriate integration time since the mean flow velocity was fluctuating with a very low frequency (≈1Hz).

From the total number of measured values only those within the limits of the standard deviation were taken. This reduced the original 1000 samples to about 800.

3.2 Boundary Layer Probe

The installation of the boundary layer probe and its support system in the TWG is shown in Fig. 3. The probe and its drive mechanism for the accurate positioning in the normal (y) and axial (x) direction was mounted on a sting which, in turn, was attached to the tunnel support generally employed to hold and vary the angle of attack of complete aircraft models. This arrangement allowed the probe to always be adjusted tangential to the model surface and traversed in the direction normal to it. The probe itself, Fig. 8, consisted of a flattened pitot probe of 0.15 mm height, a cone-cylinder static probe and a directional probe, the latter constructed of two tubes cut off under 45°. The flow direction was mainly required for the correction of the static pressure reading since the pressures indicated by the probe are dependent on the flow direction which may change considerably as the probe moves normal to the airfoil surface into the field. The probe was calibrated in the "known" flow of the TWG as function of the angle of attack and the incoming (freestream) Mach number [7].

The pressures were measured with differential pressure transducers with an accuracy

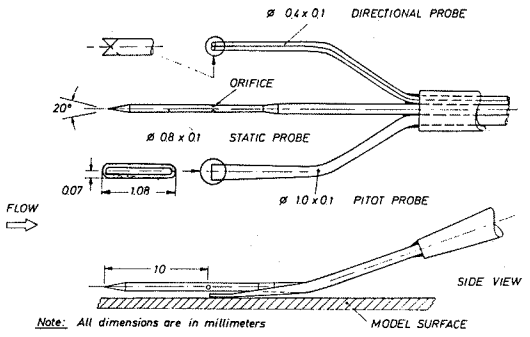

Fig. 8: Boundary layer probe.

of ±0.4% full-scale. The x-y-positions of the probe were obtained via the impulses given to the stepping motors, used to drive the probe, with an accuracy of $\Delta x/c \approx \pm 0.004$ and $\Delta y/c \approx 0.4 \times 10^{-5}$, respectively. The overall accuracy in determining the flow velocities, important in conjunction with the comparison of the probe and LDA-results, was determined to be about ±2%.

The boundary layer properties were computed from the measured static and pitot pressures assuming constant total temperature throughout the boundary layer. In determining the boundary layer integral parameters, the measured velocity profiles were supplemented by the laminar sublayer whose computation was based on the wall shear stress, τ_w, obtained by fitting a wall/wake profile to the measured data points assuming equal mass flux [7] (also see [8]). A comparison of the measured and the corresponding wall/wake profile at a position well upstream of the shock is shown in Fig. 9. It is indicated that the boundary layer profile measured at about 0.28 chord lengths downstream of the roughness band used to force transition is well represented by the law of the wall/law of the wake. The influence of adding the laminar sublayer on the determination of the boundary layer integral parameters, especially pronounced in the case of the skin friction coefficient, is depicted in Table 1.

Table 1 *Effect of adding laminar sublayer in determining boundary layer integral parameters*

	δ^*	θ	H	C_f	δ^{**}	H_{32}
Exp. data	0.320	0.138	2.314	0.00234	0.244	1.770
With sublayer	0.313	0.142	2.202	0.00281	0.250	1.759
Change [%]	-2.23	2.28	-5.09	13.52	2.40	-0.63
	mm	mm			mm	

The probe measurements must, of course, in the vicinity of separation and within separated regions be considered with caution. Since here the flow can no longer be

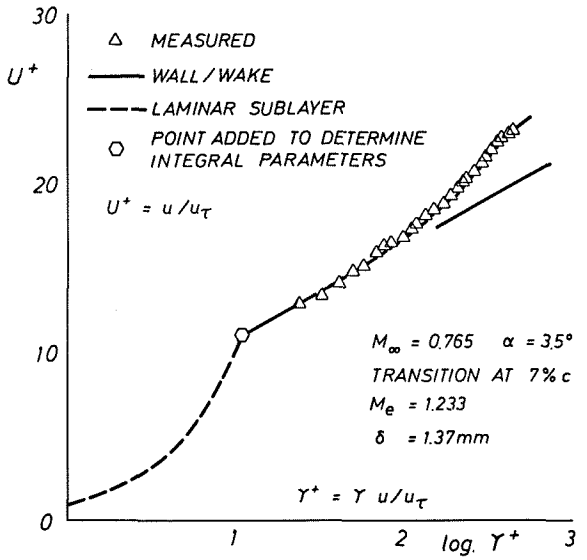

Fig. 9: Incoming boundary layer - Comparison with wall/wake law profile.

regarded as steady and reversed flow occurs, the probe reading is, particularly close to the wall, erroneous so that the boundary layer integral parameters (e.g., c_f and δ^* depicted below) are approximations showing a trend rather than absolute values. In that regard it should also be noted that the skin friction coefficients (shown in Fig. 10 and 11) were determined by a wall/wake fit to the measured data points assuming an initial value of the wall shear stress [7] [8]. In that way the onset of separation and the extent of the separated regions was reasonably well predicted.

4. DICUSSION OF RESULTS

4.1 Boundary Layer Probe Data

Emphasis in the present investigation is placed on the LDA measurements in a relatively large transonic wind tunnel at conditions of shock induced separation and on a comparison of LDA and probe results in the shock boundary layer interaction region. The discussion of some of the results of the probe measurements at this time shall merely help to identify the type of flow and boundary layer development encountered.

At the low angle of attack, the shock-upstream Mach number, representative of the shock strength, is $M_1 = 1.285$. The thickness of the incoming boundary layer is approximately $\delta = 1.5$ mm, Fig. 10. As indicated in this figure, the shock causes an increase in the boundary layer thickness by

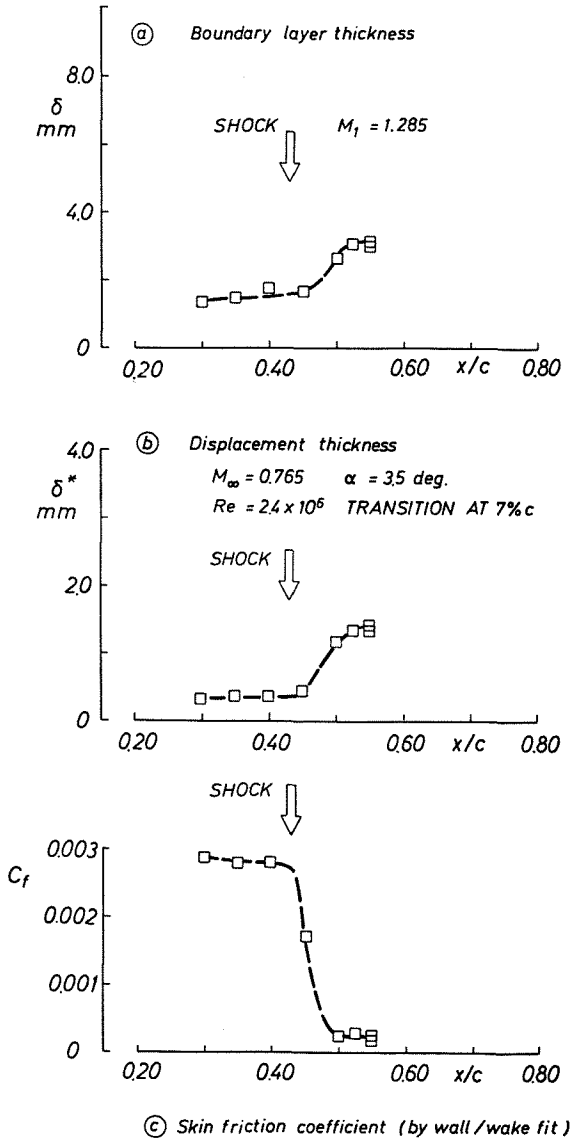

Fig. 10: Boundary layer parameters for moderate incidence.

a factor of two and an increase in the displacement thickness by a factor of about 4.4, the latter being more pronounced due to a strong retardation of the boundary layer profile close to the surface. The skin friction distribution in Fig. 10c shows that for the present shock-upstream Mach number the flow is not separated; sep-

aration is, however, likely to occur if the shock strength is slightly raised, for instance, by increasing the angle of attack.

In the second test case ($\alpha \approx 5°$), the shock-upstream Mach number is $M_1 \approx 1.36$, i.e., the shock strength is substantially higher than at the lower incidence. The corresponding boundary layer development, Fig. 11, exhibits a much more severe thickenning, with the displacement thickness now being changed by a factor of approximately 7. Furthermore, a plateau in the boundary layer parameters indicated in Fig. 10 for the low incidence case no longer exists, suggesting the presence of a large shock-induced separation bubble. The latter is confirmed by the skin friction distribution in Fig. 11c and by the Schlieren photograph of Fig. 5. The downstream extent of the separated region can, due to the aforementioned limitations of the boundary layer probe measurements, only be considered an approximation.

4.2 Laser Doppler Anemometer Results and Comparison with Probe Data.

In Fig. 12 a typical velocity profile obtained for the low- incidence test case is shown. As mentioned in Chapter 2.3, the shock position has been influenced by the probe support. Taking into account the shift in shock position of about 10%, the probe and LDA profiles have been plotted together. The agreement is quite good in the outer flow field; however, very close to the wall, the LDA data show a large amount scatter. This seems mainly due to vibrations of the model during the tests which are particularly pronounced in the mid-span of the model where the measurements took place. Also note, that the measurements were taken within the immediate shock region.

Several comparisons of boundary layer profiles obtained by LDA and the boundary layer probe for the high-incidence test case are presented in Fig. 13 to Fig. 16. Upstream (x/c = 45%) and some distance into the shock (x/c = 47% and 50%), the overall agreement between the two data sets is

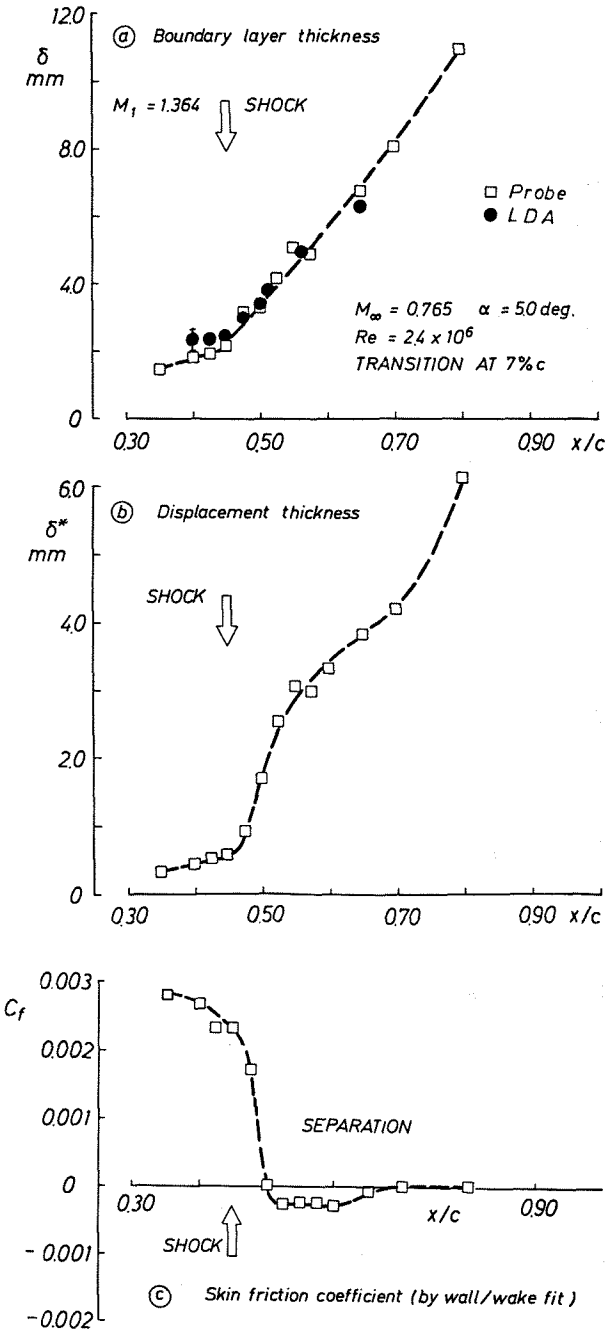

Fig.11: Boundary layer parameters for high incidence.

quite satisfactory. The LDA data scatter near the wall is less pronounced which resulted, in addition, in a better agreement - compared to $\alpha \approx 3.5$ - in the predicted boundary layer thicknesses, see Fig. 11a. At x/c = 50%, the probe data indicate the beginning of a separation bubble and a deceleration of the flow as the probe moves away from the wall through the complex lambda-shock system. The LDA data also

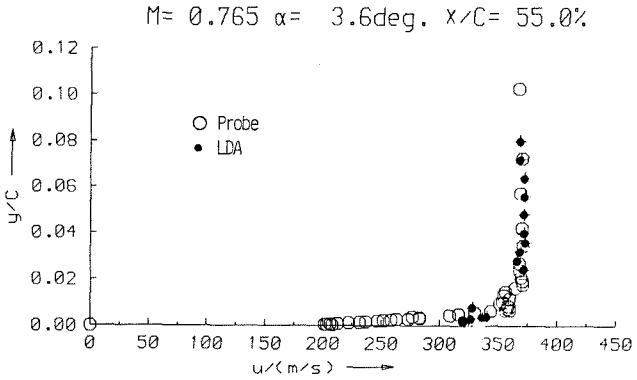

Fig.12: Velocity profile within the shock layer. Comparison probe/LDA results.
$\alpha \approx 3.6°$, x/c = 55%

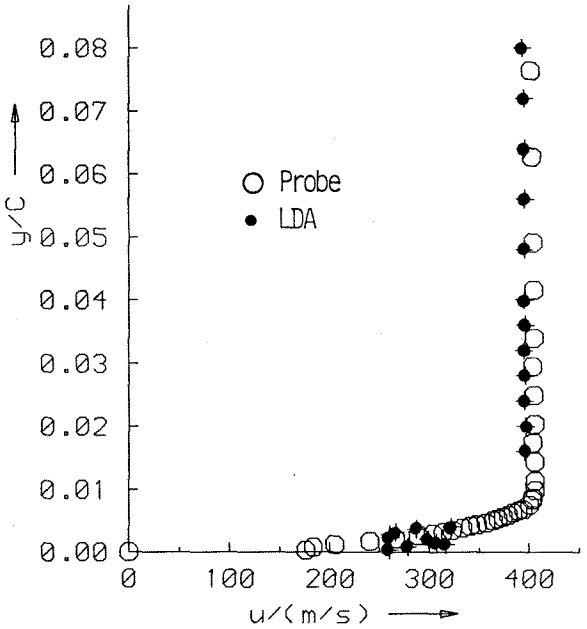

Fig.13: Velocity profiles in the shock/boundary layer interaction regime. Comparison probe/LDA results.
$\alpha \approx 5°$, x/c = 45%.

indicate the closeness to separation (also see Fig. 11c); however, the detailed outer structure is not indicated. This may be due to the intrinsic shock oscillations seen by the LDA but somewhat subdue by the presence of the probe. At x/c = 52% the outer flow is again well predicted by LDA in agreement with the probe measurement. Differences occur within the separated boundary layer. These may be due to the probe readings being erroneous at these conditions as well as the LDA not being sensitive to the flow direction since Bragg-cells were not used.

Fig. 17 shows the present LDA result for α =

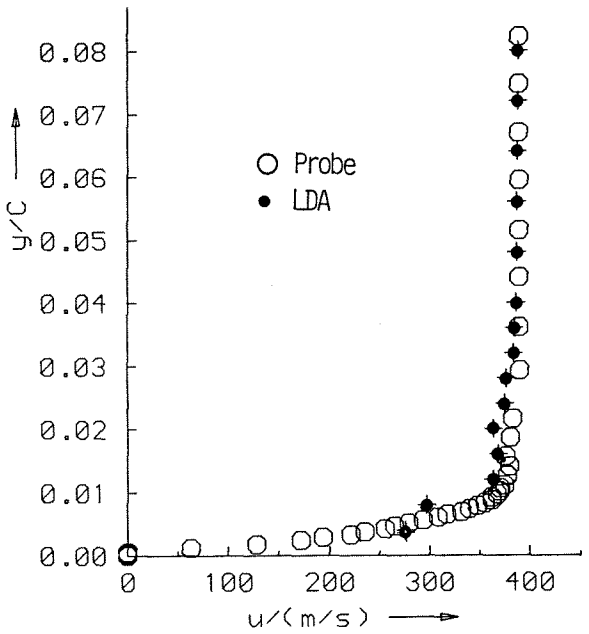

Fig.14: Velocity profiles in the shock/boundary layer interaction regime. Comparison probe/LDA results.
$\alpha \approx 5°$, x/c = 47%.

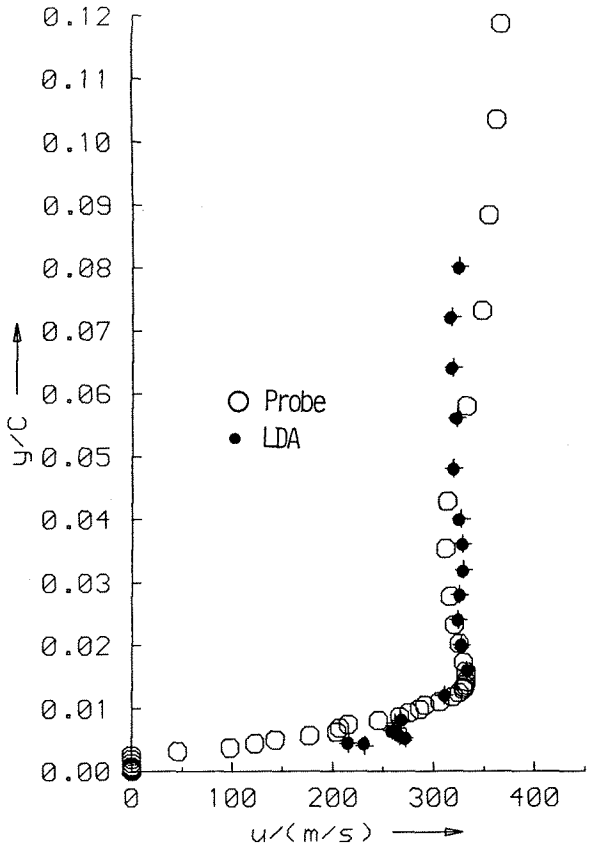

Fig.15: Velocity profiles in the shock/boundary layer interaction regime. Comparison probe/LDA results.
$\alpha \approx 5°$, x/c = 50%.

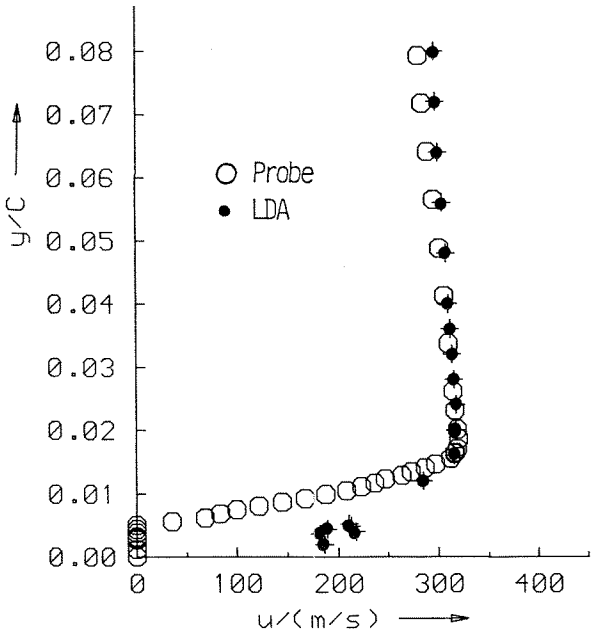

Fig.16: Velocity profiles in the shock/boundary layer interaction regime. Comparison probe/LDA results.
$\alpha \approx 5°$, x/c = 52%.

4.8° in comparison with the published LDA and probe data of Ref. 3. The velocity gradient indicated by the present data is comparable to the one shown by the 1 K LDA results, but does not confirm the steeper slope determined by the boundary layer probe. One reason may be that the position of the shock is fluctuating by a small amount and the LDA data show as a result a spreading of the pressure rise, whereas the solid pressure probe is, as mentioned earlier, fixing the shock position.
On the other hand, the distances from the wall are slightly different with the present LDA being closer to the wall where the pressure rise due to the shock is spread over a larger chordwise distance. This would also explain the lower velocities downstream of the shock. In order to demonstrate the effect of small changes in geometry, all measured velocities are presented in a 3-D carpet plot obtained by a 3-D spline interpolation, Fig. 18. Clearly, a considerable change of the velocity profile behind the shock is noted when changing from the wall from H = 4.0 (dotted line) to 5.4 mm.
The two component LDA measurements provide additional flow properties, such as the flow direction and the turbulence levels.

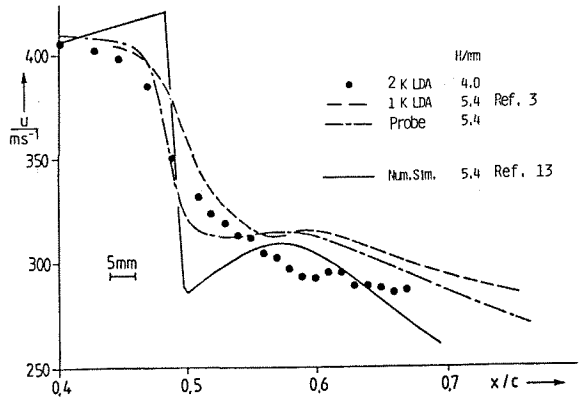

Fig.17: Velocity profiles across the shock. The two component LDA results in comparsion with results from the one component LDA, the probe measurements and with theory.

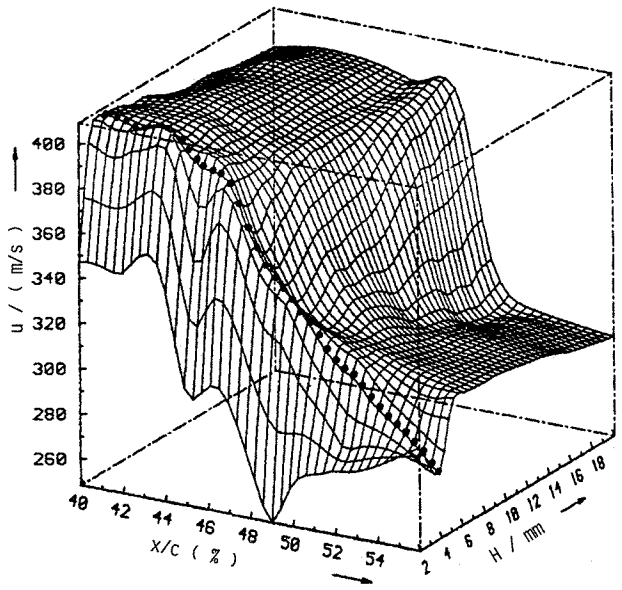

Fig.18: 3D velocity carpet plot of the two component LDA measurements.
$\alpha = 4.8°$.

Fig. 19 shows the chordwise velocity profiles across the shock for the two test cases. A pronounced change in shock structure is indicated as the angle of incidence is increased from α = 3.6° to 4.8°. In both cases the measured flow angle distribution reflects the change in the boundary layer thickness due to the intraction of the boundary layer with the shock, also indicating at the higher angle of incidence the separation region, Fig. 20. The corresponding turbulence data, which still contain some artificial noise, are pre-

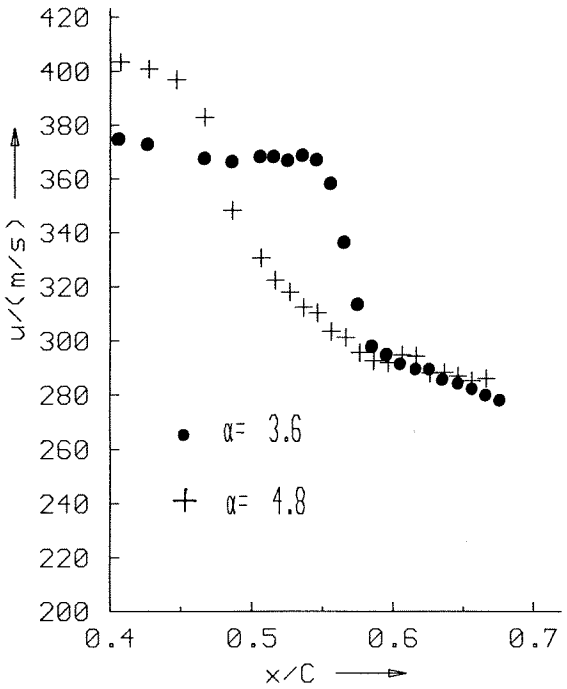

Fig.19: Chordwise velocity profiles across the shock.
$\alpha = 3.6°$ and $4.8°$.

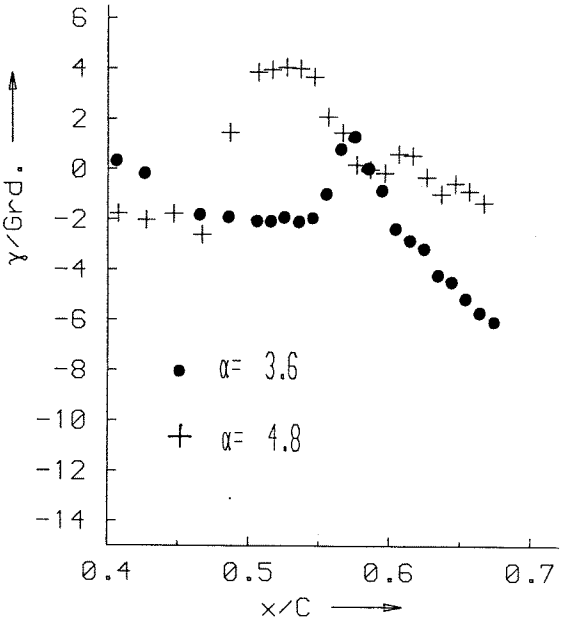

Fig.20: Change of the flow angles across the shock.
$\alpha = 3.6°$ and $4.8°$.

sented in Fig. 21. At the low incidence, the shock hardly affects turbulence. At $\alpha = 4.8°$ two regions of higher turbulence can be recognized: The first one immediately at the shock, the second associated with the reattachment process (also see Fig. 11c).

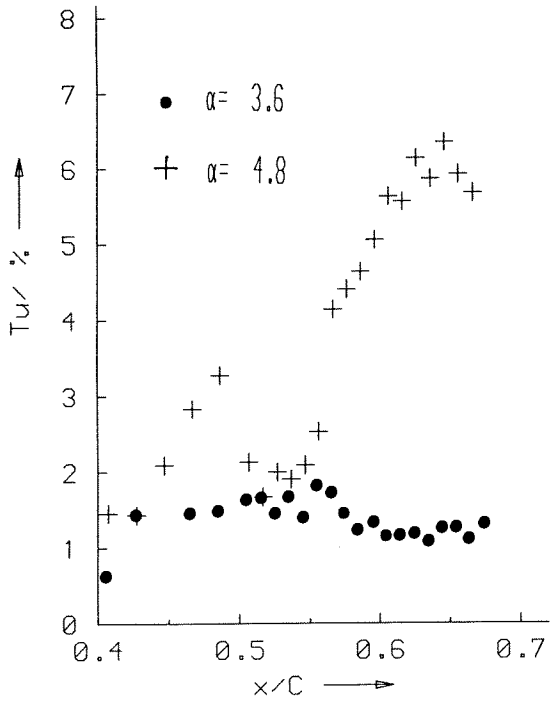

Fig.21: Turbulence profiles across the shock.
$\alpha = 3.6°$ and $4.8°$.

CONCLUSIONS

A 2D Laser Doppler Anemometer with a focal length of 750 mm and operating in backscatter mode was applied in the 1 x $1m^2$ transonic wind tunnel to analyse the shock boundary intraction region on a transonic airfoil. The LDA data were compared to conventional boundary layer probe results. Overall, the agreement between the two data sets was satisfactory. However, some discrepancies remained, especially at positions close to the wall, where the LDA data showed in some instances a considerable scatter, and within the separated region, where flow reversal occurs, and both the LDA and the probe data are suspect. As a clear advantage of the LDA one can state its ability to measure non-intrusively, thus avoiding changes, for instance, in the shock behavior, the latter obviously occurring due to the presence of the solid probe. Furthermore, more detailed information, such as turbulence level as well as the Reynolds shear stresses, can be obtained simultaneously with the

mean flow properties. The investigation has also shown that the present technique must be improved: Bragg-cells must be incorporated to determine the flow direction and, secondly, the instantaneous position of the model must be recorded and related to the position of the measuring volume.

ACKNOWLEDGEMENTS

The authors would like to thank the crew of the transonic wind tunnel TWG of the Wind Tunnel Division of DFVLR for their cooperation in performing the present test, the Engineering Department for constructing and installing the support system for the LDA and Mrs. J. Redlin and Mrs. I. Nickisch for preparing the manuscript.

5. REFERENCES

1. Stanewsky, E., and Krogmann, P., "Transonic Drag Rise and Drag Reduction by Active/Passive Boundary Layer Control", AGARD-R-723, July 1985, pp. 11-1 to 11-41.

2. Stanewsky, E., "Interaction between the Outer Inviscid Flow Field and the Boundary Layer on Transonic Airfoils", Doctoral Thesis D83, Technical University Berlin, 1981.

3. Schäfer, H.J., Horny, G., Pfeiffer, H.J. and Stanewsky, E., "Applicability of the Laser-Doppler-Anemometry to the Investigation of the Transonic Interaction between a Shock and the Boundary Layer", Deutsch-Französisches Forschungsinstitut Saint-Louis, Report R 131/83, July 1983.

4. Hottner, Th. and Lorenz-Meyer, W., "Der Transsonische Windkanal der Aerodynamischen Versuchsanstalt Göttingen (Zweite Ausbaustufe)", Jahrbuch 1968 der WGL, 1968.

5. Kühl, P. and Zimmer, H., "The Design of Airfoils for Transport Aircraft with Improved High Speed Characteristics", DORNIER GmbH.-Report 74/16 B (1974).

6. Stanewsky, E. and Zimmer, H., "Design and Wind Tunnel Testing of Three Supercritical Airfoils for Transport Aircraft", Z. Flugwiss. 23 (7/8), 1975, pp. 246-256.

7. Stanewsky, E. and Thiede, P., "Boundary Layer and Wake Measurements in the Trailing Edge Region of a Rear-loaded Transonic Airfoil", in Viscous and Interacting Flow Field Effects, German Ministry of Defense, Research Report FBWT 79-31, 1979.

8. Mathews, D.C., "Shock Wave-Boundary Layer Interactions in Two-dimensional and Axially-symmetric Flows Including the Influence of Suction", Ph.D. Thesis, University of Washington, 1969.

9. Bütefisch, K.A., Strunck, V.; A two Component LDA-System to be Operated in a 3 x 3 m^2 Low Speed Wind Tunnel. In: Proceedings of a workshop "Symposium on Applications of Laser Anemometry to Fluid Mechanics", Lisbon/Portugal, 2.-4. July, 1984.

10. Sauerland, K.-H.; Entwurf eines 3-Komponenten LDA Systems für den Transsonischen Windkanal der DLFVLR in Göttingen. LDA meeting ISL,ONERA,DFVLR, 1983

11. Adrian, R.J., Fingerson, L.M.; Laser Anemometry. Theory, Application & Technique, TSI Course, Göttingen 1981.

12. Durst, F., Melling, A., Whitelaw, I.H.; Principles and Practice of Laser Doppler Anemometry, Academic Press, 2nd edition, London, 1981

13. Niederdrenk, P., "Gleitende Stoßan - passung in schallnaher Strömung", ZAMM 62 T (1982)